Appl. Math. Mech. -Engl. Ed., **34**(4), 489–500 (2013)
DOI 10.1007/s10483-013-1685-9

Applied Mathematics and Mechanics (English Edition)

Three-dimensional flow of Oldroyd-B fluid over surface with convective boundary conditions*

T. HAYAT[1,2], S. A. SHEHZAD[1], A. ALSAEDI[2], M. S. ALHOTHUALI[2]

(1. Department of Mathematics, Quaid-i-Azam University, Islamabad 44000, Pakistan;
2. Department of Electrical and Computer Engineering, Faculty of Engineering, King Abdulaziz University, Jeddah 21589, Saudi Arabia)

Abstract The present study addresses the three-dimensional flow of an Oldroyd-B fluid over a stretching surface with convective boundary conditions. The problem formulation is presented using the conservation laws of mass, momentum, and energy. The solutions to the dimensionless problems are computed. The convergence of series solutions by the homotopy analysis method (HAM) is discussed graphically and numerically. The graphs are plotted for various parameters of the temperature profile. The series solutions are verified by providing a comparison in a limiting case. The numerical values of the local Nusselt number are analyzed.

Key words three-dimensional flow, Oldroyd-B fluid, convective boundary condition

Chinese Library Classification O373
2010 Mathematics Subject Classification 76A05

1 Introduction

Nowadays, the study of non-Newtonian fluids is a topic of great interest to the recent researchers in view of their applications in industry and technology, e.g., biological, chemical, food, and pharmaceutical industries. Several fluids such as drilling muds, shampoos, ketchup, granular suspension, apple sauce, paper pulp, slurries, paints, certain oils, polymer solutions, and clay coating are the non-Newtonian fluids. The characteristics of all non-Newtonian fluids cannot be described by a single constitutive relationship. Various fluid models were proposed in the literature to describe the properties of non-Newtonian fluids under three categories (i) differential type, (ii) rate type, and (iii) integral type. The Maxwell fluid model is the simplest class of rate type fluids. This subclass describes only the properties of relaxation time. This fluid model cannot predict the characteristics of retardation time. The Oldroyd-B fluid model was proposed to describe the properties of the relaxation time and the retardation time. Jamil et al.[1] studied the helical flows of an Oldroyd-B fluid in an infinite circular cylinder by the finite Hankel transform method. Jamil and Khan[2] investigated the flow of an Oldryd-B fluid between two coaxial cylinders. The flow in this study is induced by the inner cylinder. Sajid et al.[3] numerically investigated the boundary layer flow of an Oldroyd-B fluid in the region

* Received Apr. 16, 2012 / Revised Oct. 17, 2012
Project supported by the Deanship of Scientific Research (DSR), King Abdulaziz University, Jeddah (No. 2-135/1433HiCi)
Corresponding author S. A. SHEHZAD, E-mail: ali_qau70@yahoo.com

of stagnation point. An analysis for the two-dimensional flow of an Oldroyd-B fluid over a linearly stretched surface was carried out by Hayat and Alsaedi[4]. They discussed the effects of thermal radiation, Joule heating, and thermophoresis in this study. The magnetohydrodynamics (MHD) flow through a porous channel filled with an Oldroyd-B fluid was analyzed by Hayat et al.[5].

The stretched boundary layer flow with heat transfer has numerous applications in many engineering and industrial processes such as extrusion of plastic sheets, cooling of an infinite metallic plate in a cooling bath, spinning of fibers, drawing of plastic films, cooling of continuous strips, and aerodynamic extrusion of plastic sheets. Sakiadis[6] firstly discussed the boundary layer flow over a continuous moving surface. Crane[7] investigated the boundary layer flow over a linearly stretching surface. Since then, such problems under different aspects have been studied by various workers[8–15].

The basic aim of this paper is to investigate the three-dimensional flow of an Oldroyd-B fluid over a stretching surface in the presence of convective boundary conditions. Recently, a few researchers discussed the two-dimensional flow with convective boundary conditions. For example, Yao et al.[16] studied the two-dimensional flow of a viscous fluid with convective boundary conditions over a stretching/shrinking sheet. Blasius flow of a viscous fluid with convective boundary conditions was investigated by Aziz[17]. Flows of second grade and Maxwell fluids over a stretching surface were analyzed by Hayat et al.[18–19]. Makinde and Aziz[20] carried out a study to investigate the boundary layer flow of nanofluid with convective boundary conditions. Hence, for the three-dimensional flow, this paper is organized in the following fashion. Next section develops the mathematical formulation for the three-dimensional flow of an Oldroyd-B fluid. Section 3 has the series solutions constructed via the homotopy analysis method (HAM)[21–26]. The convergence analysis and discussion of results are presented in Section 4. Section 5 contains the main points of this study.

2 Governing problems

We consider the steady three-dimensional flow of an incompressible Oldroyd-B fluid over a stretched surface at $z = 0$. The flow takes place in the domain $z > 0$. The ambient fluid temperature is taken as T_∞, while the surface temperature is maintained by convective heat transfer at a certain value $T_{\rm f}$. The equations for the flow of the steady incompressible fluid with heat transfer are

$$\operatorname{div} V = 0, \tag{1}$$

$$\rho \frac{\mathrm{d}V}{\mathrm{d}t} = \operatorname{div} T, \tag{2}$$

in which the Cauchy stress tensor T and the extra stress tensor S are defined as

$$T = -pI + S, \tag{3}$$

$$S + \lambda_1 \frac{\mathrm{D}S}{\mathrm{D}t} = \mu\Big(A_1 + \lambda_2 \frac{\mathrm{D}A_1}{\mathrm{D}t}\Big), \tag{4}$$

$$(V \cdot \nabla)T = \sigma \nabla^2 T, \tag{5}$$

where $\frac{\mathrm{D}}{\mathrm{D}t}$ is the covariant differentiation, and λ_1 and λ_2 are the relaxation time and the retardation time, respectively. The first Rivlin Ericksen tensor A_1 is defined as

$$A_1 = \operatorname{grad} V + (\operatorname{grad} V)^*,$$

where * indicates the matrix transpose, and the velocity field V is taken as

$$V = (u(x,y,z), v(x,y,z), w(x,y,z)). \tag{6}$$

The definition of $\frac{\mathrm{D}}{\mathrm{D}t}$ is[27]

$$\frac{\mathrm{D}a_i}{\mathrm{D}t} = \frac{\partial a_i}{\partial t} + u_r a_{i,r} - u_{i,r} a_r. \tag{7}$$

Following the procedure of Ref. [27] at pages 221–223, Eqs. (1)–(5) now give

$$\frac{\partial u}{\partial x} + \frac{\partial v}{\partial y} + \frac{\partial w}{\partial z} = 0, \tag{8}$$

$$\begin{aligned}
&u\frac{\partial u}{\partial x} + v\frac{\partial u}{\partial y} + w\frac{\partial u}{\partial z} + \lambda_1\Big(u^2\frac{\partial^2 u}{\partial x^2} + v^2\frac{\partial^2 u}{\partial y^2} + w^2\frac{\partial^2 u}{\partial z^2} + 2uv\frac{\partial^2 u}{\partial x\partial y} + 2vw\frac{\partial^2 u}{\partial y\partial z} + 2uw\frac{\partial^2 u}{\partial x\partial z}\Big)\\
=& -\frac{\partial p}{\partial x} + \nu\Big(\frac{\partial^2 u}{\partial x^2} + \frac{\partial^2 u}{\partial y^2} + \frac{\partial^2 u}{\partial z^2} + \lambda_2\Big(u\frac{\partial^3 u}{\partial x^3} + u\frac{\partial^3 u}{\partial x\partial y^2} + u\frac{\partial^3 u}{\partial x\partial z^2} + v\frac{\partial^3 u}{\partial x^2\partial y}\\
&+ u\frac{\partial^3 u}{\partial y^3} + v\frac{\partial^3 u}{\partial y\partial z^2} + w\frac{\partial^3 u}{\partial x^2\partial z} + w\frac{\partial^3 u}{\partial y^2\partial z} + w\frac{\partial^3 u}{\partial z^3} - \frac{\partial u}{\partial x}\frac{\partial^2 u}{\partial x^2} - \frac{\partial u}{\partial x}\frac{\partial^2 u}{\partial y^2}\\
&- \frac{\partial u}{\partial x}\frac{\partial^2 u}{\partial z^2} - \frac{\partial u}{\partial y}\frac{\partial^2 v}{\partial x^2} - \frac{\partial u}{\partial y}\frac{\partial^2 v}{\partial y^2} - \frac{\partial u}{\partial y}\frac{\partial^2 v}{\partial z^2} - \frac{\partial u}{\partial z}\frac{\partial^2 w}{\partial x^2} - \frac{\partial u}{\partial z}\frac{\partial^2 w}{\partial y^2} - \frac{\partial u}{\partial z}\frac{\partial^2 w}{\partial z^2}\Big)\Big),
\end{aligned} \tag{9}$$

$$\begin{aligned}
&u\frac{\partial v}{\partial x} + v\frac{\partial v}{\partial y} + w\frac{\partial v}{\partial z} + \lambda_1\Big(u^2\frac{\partial^2 v}{\partial x^2} + v^2\frac{\partial^2 v}{\partial y^2} + w^2\frac{\partial^2 v}{\partial z^2} + 2uv\frac{\partial^2 v}{\partial x\partial y} + 2vw\frac{\partial^2 v}{\partial y\partial z} + 2uw\frac{\partial^2 v}{\partial x\partial z}\Big)\\
=& -\frac{\partial p}{\partial y} + \nu\Big(\frac{\partial^2 v}{\partial x^2} + \frac{\partial^2 v}{\partial y^2} + \frac{\partial^2 v}{\partial z^2} + \lambda_2\Big(u\frac{\partial^3 v}{\partial x^3} + u\frac{\partial^3 v}{\partial x\partial y^2} + u\frac{\partial^3 v}{\partial x\partial z^2} + v\frac{\partial^3 v}{\partial x^2\partial y}\\
&+ v\frac{\partial^3 v}{\partial y^3} + v\frac{\partial^3 v}{\partial y\partial z^2} + w\frac{\partial^3 v}{\partial x^2\partial z} + w\frac{\partial^3 v}{\partial y^2\partial z} + w\frac{\partial^3 v}{\partial z^3} - \frac{\partial v}{\partial x}\frac{\partial^2 u}{\partial x^2} - \frac{\partial v}{\partial x}\frac{\partial^2 u}{\partial y^2}\\
&- \frac{\partial v}{\partial x}\frac{\partial^2 u}{\partial z^2} - \frac{\partial v}{\partial y}\frac{\partial^2 v}{\partial x^2} - \frac{\partial v}{\partial y}\frac{\partial^2 v}{\partial y^2} - \frac{\partial v}{\partial y}\frac{\partial^2 v}{\partial z^2} - \frac{\partial v}{\partial z}\frac{\partial^2 w}{\partial x^2} - \frac{\partial v}{\partial z}\frac{\partial^2 w}{\partial y^2} - \frac{\partial v}{\partial z}\frac{\partial^2 w}{\partial z^2}\Big)\Big),
\end{aligned} \tag{10}$$

$$\begin{aligned}
&u\frac{\partial w}{\partial x} + v\frac{\partial w}{\partial y} + w\frac{\partial w}{\partial z} + \lambda_1\Big(u^2\frac{\partial^2 w}{\partial x^2} + v^2\frac{\partial^2 w}{\partial y^2} + w^2\frac{\partial^2 w}{\partial z^2} + 2uv\frac{\partial^2 w}{\partial x\partial y} + 2vw\frac{\partial^2 w}{\partial y\partial z} + 2uw\frac{\partial^2 w}{\partial x\partial z}\Big)\\
=& -\frac{\partial p}{\partial z} + \nu\Big(\frac{\partial^2 w}{\partial x^2} + \frac{\partial^2 w}{\partial y^2} + \frac{\partial^2 w}{\partial z^2} + \lambda_2\Big(u\frac{\partial^3 w}{\partial x^3} + u\frac{\partial^3 w}{\partial x\partial y^2} + u\frac{\partial^3 w}{\partial x\partial z^2} + v\frac{\partial^3 w}{\partial x^2\partial y}\\
&+ v\frac{\partial^3 w}{\partial y^3} + v\frac{\partial^3 w}{\partial y\partial z^2} + w\frac{\partial^3 w}{\partial x^2\partial z} + w\frac{\partial^3 w}{\partial y^2\partial z} + w\frac{\partial^3 w}{\partial z^3} - \frac{\partial w}{\partial x}\frac{\partial^2 u}{\partial x^2} - \frac{\partial w}{\partial x}\frac{\partial^2 u}{\partial y^2}\\
&- \frac{\partial w}{\partial x}\frac{\partial^2 u}{\partial z^2} - \frac{\partial w}{\partial y}\frac{\partial^2 v}{\partial x^2} - \frac{\partial w}{\partial y}\frac{\partial^2 v}{\partial y^2} - \frac{\partial w}{\partial y}\frac{\partial^2 v}{\partial z^2} - \frac{\partial w}{\partial z}\frac{\partial^2 w}{\partial x^2} - \frac{\partial w}{\partial z}\frac{\partial^2 w}{\partial y^2} - \frac{\partial w}{\partial z}\frac{\partial^2 w}{\partial z^2}\Big)\Big),
\end{aligned} \tag{11}$$

$$u\frac{\partial T}{\partial x} + v\frac{\partial T}{\partial y} + w\frac{\partial T}{\partial z} = \sigma\Big(\frac{\partial^2 T}{\partial x^2} + \frac{\partial^2 T}{\partial y^2} + \frac{\partial^2 T}{\partial z^2}\Big). \tag{12}$$

After neglecting the pressure gradient and using the standard boundary layer assumptions[28], the resulting aligns for the three-dimensional flow of an Oldroyd-B fluid are

$$\begin{aligned}
&u\frac{\partial u}{\partial x} + v\frac{\partial u}{\partial y} + w\frac{\partial u}{\partial z} + \lambda_1\Big(u^2\frac{\partial^2 u}{\partial x^2} + v^2\frac{\partial^2 u}{\partial y^2} + w^2\frac{\partial^2 u}{\partial z^2} + 2uv\frac{\partial^2 u}{\partial x\partial y} + 2vw\frac{\partial^2 u}{\partial y\partial z} + 2uw\frac{\partial^2 u}{\partial x\partial z}\Big)\\
=&\,\nu\Big(\frac{\partial^2 u}{\partial z^2} + \lambda_2\Big(u\frac{\partial^3 u}{\partial x\partial z^2} + v\frac{\partial^3 u}{\partial y\partial z^2} + w\frac{\partial^3 u}{\partial z^3} - \frac{\partial u}{\partial x}\frac{\partial^2 u}{\partial z^2} - \frac{\partial u}{\partial y}\frac{\partial^2 v}{\partial z^2} - \frac{\partial u}{\partial z}\frac{\partial^2 w}{\partial z^2}\Big)\Big),
\end{aligned} \tag{13}$$

$$u\frac{\partial v}{\partial x}+v\frac{\partial v}{\partial y}+w\frac{\partial v}{\partial z}+\lambda_1\Big(u^2\frac{\partial^2 v}{\partial x^2}+v^2\frac{\partial^2 v}{\partial y^2}+w^2\frac{\partial^2 v}{\partial z^2}+2uv\frac{\partial^2 v}{\partial x\partial y}+2vw\frac{\partial^2 v}{\partial y\partial z}+2uw\frac{\partial^2 v}{\partial x\partial z}\Big)$$
$$=\nu\Big(\frac{\partial^2 v}{\partial z^2}+\lambda_2\Big(u\frac{\partial^3 v}{\partial x\partial z^2}+v\frac{\partial^3 v}{\partial y\partial z^2}+w\frac{\partial^3 v}{\partial z^3}-\frac{\partial v}{\partial x}\frac{\partial^2 v}{\partial z^2}-\frac{\partial v}{\partial y}\frac{\partial^2 v}{\partial z^2}-\frac{\partial v}{\partial z}\frac{\partial^2 w}{\partial z^2}\Big)\Big), \tag{14}$$

$$u\frac{\partial T}{\partial x}+v\frac{\partial T}{\partial y}+w\frac{\partial T}{\partial z}=\sigma\frac{\partial^2 T}{\partial z^2}, \tag{15}$$

where the respective velocity components in the x-, y-, and z-directions are denoted by u, v, and w, λ_1 and λ_2 show the relaxation and retardation times, respectively, T is the fluid temperature, σ is the thermal diffusivity of the fluid, $\nu=\frac{\mu}{\rho}$ is the kinematic viscosity, μ is the dynamic viscosity of fluid, and ρ is the density of fluid. Note that Eq. (11) is identically satisfied through the boundary layer approximation and in absence of the pressure gradient.

The convective boundary conditions are

$$u=ax,\quad v=by,\quad w=0,\quad -k\frac{\partial T}{\partial z}=h(T_{\mathrm{f}}-T)\quad \text{at}\quad z=0, \tag{16}$$

$$u\to 0,\quad v\to 0,\quad T\to T_\infty\quad \text{as}\quad z\to\infty, \tag{17}$$

where k indicates the thermal conductivity of fluid, and a and b have the dimension inverses of time.

Using the following new variables:

$$\begin{cases} u=axf'(\eta),\quad v=ayg'(\eta),\quad w=-\sqrt{a\nu}(f(\eta)+g(\eta)),\\ \theta(\eta)=\dfrac{T-T_\infty}{T_{\mathrm{f}}-T_\infty},\quad \eta=z\sqrt{\dfrac{a}{\nu}}, \end{cases} \tag{18}$$

Eq. (8) is satisfied automatically, and Eqs. (13)–(15) give

$$f'''+(f+g)f''-f'^2+\beta_1(2(f+g)f'f''-(f+g)^2f''')+\beta_2((f''+g'')f''-(f+g)f'''')=0, \tag{19}$$

$$g'''+(f+g)g''-g'^2+\beta_1(2(f+g)g'g''-(f+g)^2g''')+\beta_2((f''+g'')g''-(f+g)g'''')=0, \tag{20}$$

$$\theta''+Pr(f+g)\theta'=0, \tag{21}$$

$$f=0,\quad g=0,\quad f'=1,\quad g'=\beta,\quad \theta'=-\gamma(1-\theta(0))\quad \text{at}\quad \eta=0, \tag{22}$$

$$f'\to 0,\quad g'\to 0,\quad \theta\to 0\quad \text{as}\quad \eta\to\infty, \tag{23}$$

where $\beta_1=\lambda_1 a$ and $\beta_2=\lambda_2 a$ are the Deborah numbers, $\beta=\frac{b}{a}$ is a parameter, $Pr=\frac{\nu}{\sigma}$ is the Prandtl number, $\gamma=\frac{h}{k}\sqrt{\frac{\nu}{a}}$ is the Biot number, and the prime shows the differentiation with respect to η.

The expression for the local Nusselt number with heat transfer q_{w} is

$$\begin{cases} Nu_x=\dfrac{xq_{\mathrm{w}}}{k(T_{\mathrm{f}}-T_\infty)},\\ q_{\mathrm{w}}=-k\Big(\dfrac{\partial T}{\partial z}\Big)_{z=0}. \end{cases} \tag{24}$$

In the dimensionless form, the above equation can be written as

$$\frac{Nu_x}{Re_x^{\frac{1}{2}}}=-\theta'(0), \tag{25}$$

in which $Re_x=\frac{ux}{\nu}$ is the local Reynolds number.

3 Series solutions

The initial approximations and the auxiliary linear operators for the homotopy analysis solutions are chosen as

$$f_0(\eta) = 1 - \exp(-\eta), \quad g_0(\eta) = \beta(1 - \exp(-\eta)), \quad \theta_0(\eta) = \frac{\gamma \exp(-\eta)}{1+\gamma}, \tag{26}$$

$$\mathcal{L}_f = f''' - f', \quad \mathcal{L}_g = g''' - g', \quad \mathcal{L}_\theta = \theta'' - \theta. \tag{27}$$

We note that the auxiliary linear operators in the above equation satisfy the following properties:

$$\begin{cases} \mathcal{L}_f(C_1 + C_2 \mathrm{e}^{\eta} + C_3 \mathrm{e}^{-\eta}) = 0, \\ \mathcal{L}_g(C_4 + C_5 \mathrm{e}^{\eta} + C_6 \mathrm{e}^{-\eta}) = 0, \\ \mathcal{L}_\theta(C_7 \mathrm{e}^{\eta} + C_8 \mathrm{e}^{-\eta}) = 0, \end{cases} \tag{28}$$

where C_i $(i = 1, 2, \cdots, 8)$ are the arbitrary constants.

The associated zeroth-order deformation problems are

$$(1-p)\mathcal{L}_f(\widehat{f}(\eta;p) - f_0(\eta)) = p\hbar_f \mathcal{N}_f(\widehat{f}(\eta;p), \widehat{g}(\eta;p)), \tag{29}$$

$$(1-p)\mathcal{L}_g(\widehat{g}(\eta;p) - g_0(\eta)) = p\hbar_g \mathcal{N}_g(\widehat{f}(\eta;p), \widehat{g}(\eta;p)), \tag{30}$$

$$(1-p)\mathcal{L}_\theta(\widehat{\theta}(\eta;p) - \theta_0(\eta)) = p\hbar_\theta \mathcal{N}_\theta(\widehat{f}(\eta;p), \widehat{g}(\eta;p), \widehat{\theta}(\eta,p)), \tag{31}$$

$$\begin{cases} \widehat{f}(0;p) = 0, \quad \widehat{f}'(0;p) = 1, \quad \widehat{f}'(\infty;p) = 0, \quad \widehat{g}(0;p) = 0, \quad \widehat{g}'(0;p) = \beta, \\ \widehat{g}'(\infty;p) = 0, \quad \widehat{\theta}'(0,p) = -\gamma(1 - \theta(0,p)), \quad \widehat{\theta}(\infty,p) = 0, \end{cases} \tag{32}$$

$$\begin{aligned} \mathcal{N}_f(\widehat{f}(\eta,p), \widehat{g}(\eta,p)) = {} & \frac{\partial^3 \widehat{f}(\eta,p)}{\partial \eta^3} - \Big(\frac{\partial \widehat{f}(\eta,p)}{\partial \eta}\Big)^2 + (\widehat{f}(\eta,p) + \widehat{g}(\eta,p))\frac{\partial^2 \widehat{f}(\eta,p)}{\partial \eta^2} \\ & + \beta_1\Big(2(\widehat{f}(\eta,p) + \widehat{g}(\eta,p))\frac{\partial \widehat{f}(\eta,p)}{\partial \eta}\frac{\partial^2 \widehat{f}(\eta,p)}{\partial \eta^2} \\ & - (\widehat{f}(\eta,p) + \widehat{g}(\eta,p))^2 \frac{\partial^3 \widehat{f}(\eta,p)}{\partial \eta^2}\Big) \\ & + \beta_2\Big(\Big(\frac{\partial^2 \widehat{f}(\eta,p)}{\partial \eta^2} + \frac{\partial^2 \widehat{g}(\eta,p)}{\partial \eta^2}\Big)\frac{\partial^2 \widehat{f}(\eta,p)}{\partial \eta^2} \\ & - (\widehat{f}(\eta,p) + \widehat{g}(\eta,p))\frac{\partial^4 \widehat{f}(\eta,p)}{\partial \eta^4}\Big), \end{aligned} \tag{33}$$

$$\begin{aligned} \mathcal{N}_g(\widehat{g}(\eta,p), \widehat{f}(\eta,p)) = {} & \frac{\partial^3 \widehat{g}(\eta,p)}{\partial \eta^3} - \Big(\frac{\partial \widehat{g}(\eta,p)}{\partial \eta}\Big)^2 + (\widehat{f}(\eta,p) + \widehat{g}(\eta,p))\frac{\partial^2 \widehat{g}(\eta,p)}{\partial \eta^2} \\ & + \beta_1\Big(2(\widehat{f}(\eta,p) + \widehat{g}(\eta,p))\frac{\partial \widehat{g}(\eta,p)}{\partial \eta}\frac{\partial^2 \widehat{g}(\eta,p)}{\partial \eta^2} \\ & - (\widehat{f}(\eta,p) + \widehat{g}(\eta,p))^2 \frac{\partial^3 \widehat{g}(\eta,p)}{\partial \eta^2}\Big) \end{aligned}$$

$$+\beta_2\Big(\Big(\frac{\partial^2\widehat{f}(\eta,p)}{\partial\eta^2}+\frac{\partial^2\widehat{g}(\eta,p)}{\partial\eta^2}\Big)\frac{\partial^2\widehat{g}(\eta,p)}{\partial\eta^2} - (\widehat{f}(\eta,p)+\widehat{g}(\eta,p))\frac{\partial^4\widehat{g}(\eta,p)}{\partial\eta^4}\Big), \tag{34}$$

$$\mathcal{N}_\theta(\widehat{\theta}(\eta,p),\widehat{f}(\eta,p),\widehat{g}(\eta,p))=\frac{\partial^2\widehat{\theta}(\eta,p)}{\partial\eta^2}+Pr(\widehat{f}(\eta,p)+\widehat{g}(\eta,p))\frac{\partial\widehat{\theta}(\eta,p)}{\partial\eta}. \tag{35}$$

Here, p is an embedding parameter, $\hbar_f$, $\hbar_g$, and $\hbar_\theta$ are the non-zero auxiliary parameters, and $\mathcal{N}_f$, $\mathcal{N}_g$, and $\mathcal{N}_\theta$ indicate the nonlinear operators. For $p=0$ and $p=1$, we have

$$\widehat{f}(\eta;0)=f_0(\eta),\quad \widehat{\theta}(\eta,0)=\theta_0(\eta),\quad \widehat{f}(\eta;1)=f(\eta),\quad \widehat{\theta}(\eta,1)=\theta(\eta). \tag{36}$$

Further, when p increases from 0 to 1, $f(\eta,p)$, $g(\eta,p)$, and $\theta(\eta,p)$ vary from $f_0(\eta)$, $g_0(\eta)$, and $\theta_0(\eta)$ to $f(\eta)$, $g(\eta)$, and $\theta(\eta)$. Using Taylor's series expansion, one can write

$$f(\eta,p)=f_0(\eta)+\sum_{m=1}^{\infty}f_m(\eta)p^m,\quad f_m(\eta)=\frac{1}{m!}\frac{\partial^m f(\eta;p)}{\partial\eta^m}\Big|_{p=0}, \tag{37}$$

$$g(\eta,p)=g_0(\eta)+\sum_{m=1}^{\infty}g_m(\eta)p^m,\quad g_m(\eta)=\frac{1}{m!}\frac{\partial^m g(\eta;p)}{\partial\eta^m}\Big|_{p=0}, \tag{38}$$

$$\theta(\eta,p)=\theta_0(\eta)\sum_{m=1}^{\infty}\theta_m(\eta)p^m,\quad \theta_m(\eta)=\frac{1}{m!}\frac{\partial^m \theta(\eta;p)}{\partial\eta^m}\Big|_{p=0}, \tag{39}$$

where the convergence of above series strongly depends upon $\hbar_f$, $\hbar_g$, and $\hbar_\theta$. Consider that $\hbar_f$, $\hbar_g$, and $\hbar_\theta$ are selected properly so that Eqs. (29)–(31) converge at $p=1$. Therefore,

$$f(\eta)=f_0(\eta)+\sum_{m=1}^{\infty}f_m(\eta), \tag{40}$$

$$g(\eta)=g_0(\eta)+\sum_{m=1}^{\infty}g_m(\eta), \tag{41}$$

$$\theta(\eta)=\theta_0(\eta)+\sum_{m=1}^{\infty}\theta_m(\eta). \tag{42}$$

The general solutions can be expressed as

$$f_m(\eta)=f_m^*(\eta)+C_1+C_2\mathrm{e}^{\eta}+C_3\mathrm{e}^{-\eta}, \tag{43}$$

$$g_m(\eta)=g_m^*(\eta)+C_4+C_5\mathrm{e}^{\eta}+C_6\mathrm{e}^{-\eta}, \tag{44}$$

$$\theta_m(\eta)=\theta_m^*(\eta)+C_7\mathrm{e}^{\eta}+C_8\mathrm{e}^{-\eta}, \tag{45}$$

in which f_m^*, g_m^*, and θ_m^* indicate the special solutions.

4 Convergence analysis and discussion of results

We note that the series (40)–(42) have the auxiliary parameters $\hbar_f$, $\hbar_g$, and $\hbar_\theta$. These parameters have a key role to adjust and control the convergence of series solutions. The $\hbar$-curves have been sketched at the 18th-order of approximations to determine the suitable ranges for $\hbar_f$, $\hbar_g$, and $\hbar_\theta$. Figure 1 shows that the ranges of admissible values of $\hbar_f$, $\hbar_g$, and $\hbar_\theta$ are $-1.30 \leqslant \hbar_f \leqslant -0.30$, $-1.30 \leqslant \hbar_g \leqslant -0.25$, and $-1.40 \leqslant \hbar_\theta \leqslant -0.45$. We observe that our series solutions converge in the whole region of η when $\hbar_f = \hbar_g = \hbar_\theta = -0.6$ (see Table 1).

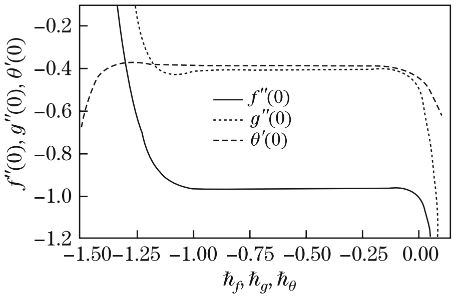

Fig. 1 $\hbar$-curves for functions f, g, and θ when $\beta_1 = 0.3, \beta_2 = 0.4, Pr = 1.0, \gamma = 0.8$, and $\beta = 0.5$

Table 1 Convergence of series solutions for different orders of approximation when $\beta_1 = 0.3$, $\beta_2 = 0.4$, $Pr = 1.0$, $\gamma = 0.8$, $\beta = 0.5$, and $\hbar_f = \hbar_g = \hbar_\theta = -0.6$

Order of approximation	$-f''(0)$	$-g''(0)$	$-\theta'(0)$
1	0.948 75	0.413 13	0.414 81
10	0.964 60	0.406 14	0.387 71
15	0.964 49	0.406 19	0.387 91
20	0.964 50	0.406 22	0.387 90
25	0.964 50	0.406 22	0.387 90
30	0.964 50	0.406 22	0.387 90
35	0.964 50	0.406 22	0.387 90

Figures 2–13 are plotted to see the variations of the Deborah numbers β_1 and β_2, the Prandtl number Pr, and the Biot number γ on the fluid temperature $\theta(\eta)$ when $\beta=0.0$, $\beta=0.5$, and $\beta=1.0$. Figure 2 illustrates the effect of the Deborah number β_1 on the temperature field for $\beta=0.0$. Here, both the fluid temperature and thermal boundary layer thickness increase by increasing β_1. Physically, this is due to the fact that the Deborah number β_1 contains the relaxation time λ_1. The increase in the relaxation time leads to the increases in the temperature and the thermal boundary layer thickness. Figure 3 shows the influence of the Deborah number β_2 on the temperature field when $\beta=0.0$. The effects of β_2 on the temperature and the thermal boundary layer thickness are opposite to those of β_1. This is due to the reason that the retardation time provides resistance which causes reduction in the temperature and the thermal boundary layer thickness. Figure 4 clearly depicts that the larger Prandtl number corresponds to the lower temperature and thermal boundary layer thickness. In fact, the larger Prandtl number means that the thermal diffusivity is lower. A decrease in the thermal diffusivity leads to a decrease in the temperature and its associated boundary layer thickness. Figure 5 presents the variations of the Biot number on the temperature profile for $\beta = 0.0$. An increase in the Biot number gives rise to the temperature and the thermal boundary layer thickness. We also observe that the temperature and the thermal boundary layer thickness are increasing functions of the Biot number. Further, it is noticed that the peak temperature occurs in the thermal boundary layer in the region near the surface. Figures 6–9 are plotted to see the influences of different parameters on the temperature $\theta(\eta)$ for $\beta=0.5$. From Fig. 6, one can see that β_1 has the same effects on the temperature as in the case of $\beta=0.0$. The only difference we noticed is that the increase in the temperature is more dominant for $\beta=0.5$ in comparison to $\beta=0.0$. By making a comparison of Figs. 3 and 7, we conclude that β_2 has a similar effect for $\beta=0.0$ and

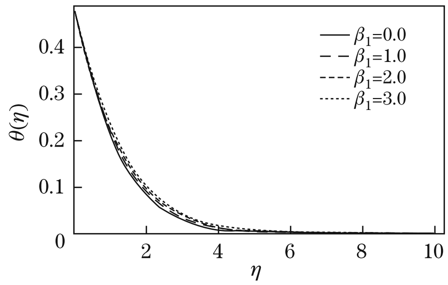

Fig. 2 Influence of β_1 on $\theta(\eta)$ when $\beta = 0.0$, $Pr = 1.0, \beta_2 = 0.4$, and $\gamma = 0.6$

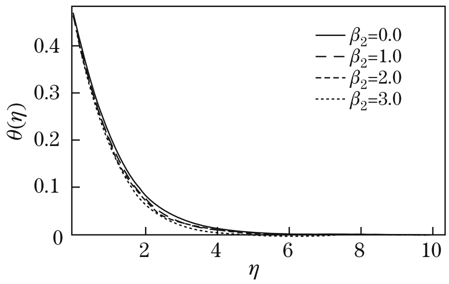

Fig. 3 Influence of β_2 on $\theta(\eta)$ when $\beta = 0.0$, $Pr = 1.0, \beta_1 = 0.4$, and $\gamma = 0.6$

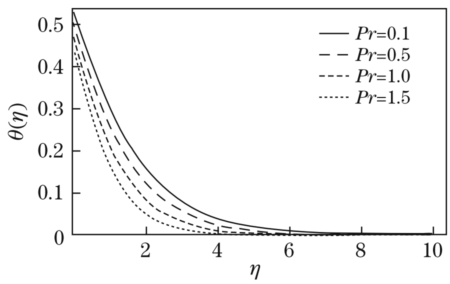

Fig. 4 Influence of Pr on $\theta(\eta)$ when $\beta = 0.0$, $\beta_1 = \beta_2 = 0.4$, and $\gamma = 0.6$

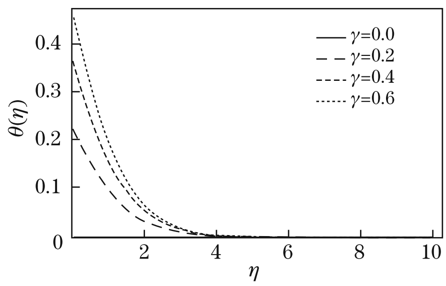

Fig. 5 Influence of γ on $\theta(\eta)$ when $\beta = 0.0$, $Pr = 1.0$, and $\beta_1 = \beta_2 = 0.4$

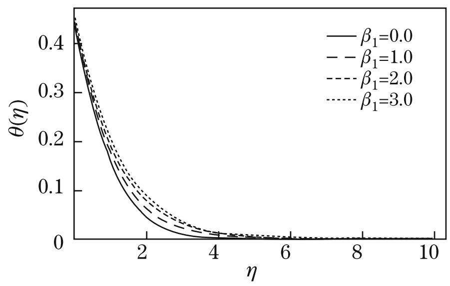

Fig. 6 Influence of β_1 on $\theta(\eta)$ when $\beta = 0.5$, $Pr = 1.0, \beta_2 = 0.4$, and $\gamma = 0.6$

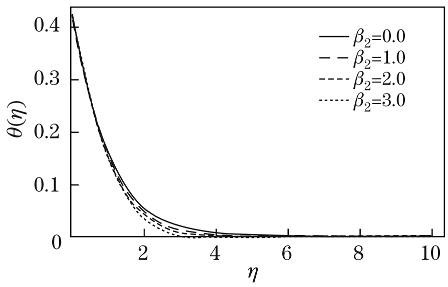

Fig. 7 Influence of β_2 on $\theta(\eta)$ when $\beta = 0.5$, $Pr = 1.0, \beta_1 = 0.4$, and $\gamma = 0.6$

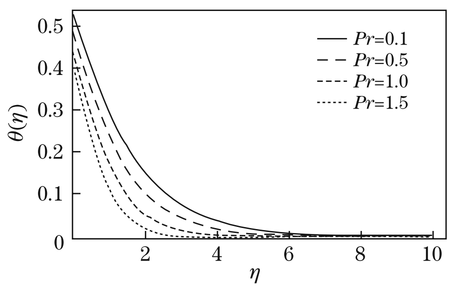

Fig. 8 Influence of Pr on $\theta(\eta)$ when $\beta = 0.5$, $\beta_1 = \beta_2 = 0.4$, and $\gamma = 0.6$

$\beta = 0.5$. Figure 8 clearly shows that the variations in the temperature due to an increase in the Prandtl number for $\beta = 0.5$ are large when compared with $\beta = 0.0$. The effects of the Biot number on the temperature are similar in a qualitative sense (see Figs. 5 and 9). Figure 10 is plotted to see the effects of β_1 on the temperature for $\beta = 1.0$. It shows that the fluid temperature and the thermal boundary layer thickness are increasing functions of β_1 for $\beta = 1.0$. There is a decrease in the temperature and the thermal boundary layer thickness with an increase in β_2 for $\beta = 1.0$. The effects of the Prandtl and Biot numbers on the fluid temperature are similar to those of $\beta = 0.0$ and $\beta = 0.5$. Figure 14 is prepared to analyze the variations of the stretching parameter on the fluid temperature. We can see that the fluid temperature and thermal boundary layer thickness reduce with an increase in β.

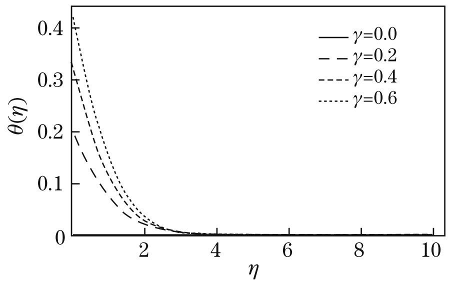

Fig. 9 Influence of γ on $\theta(\eta)$ when $\beta = 0.5$, $Pr = 1.0$, and $\beta_1 = \beta_2 = 0.4$

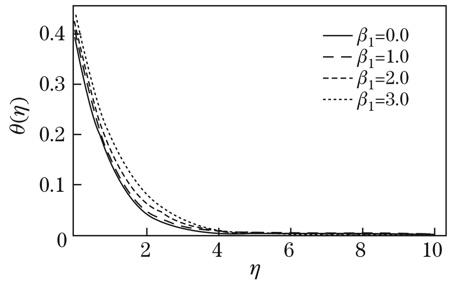

Fig. 10 Influence of β_1 on $\theta(\eta)$ when $\beta = 1.0$, $Pr = 1.0, \beta_2 = 0.4$, and $\gamma = 0.6$

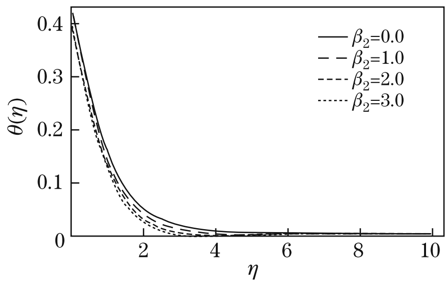

Fig. 11 Influence of β_2 on $\theta(\eta)$ when $\beta = 1.0$, $Pr = 1.0, \beta_1 = 0.4$, and $\gamma = 0.6$

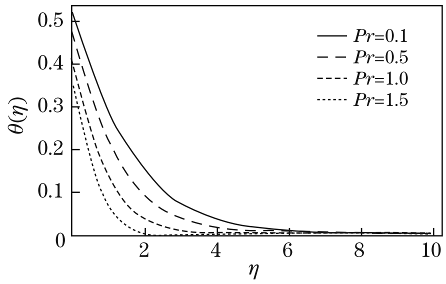

Fig. 12 Influence of Pr on $\theta(\eta)$ when $\beta = 1.0$, $\beta_1 = \beta_2 = 0.4$, and $\gamma = 0.6$

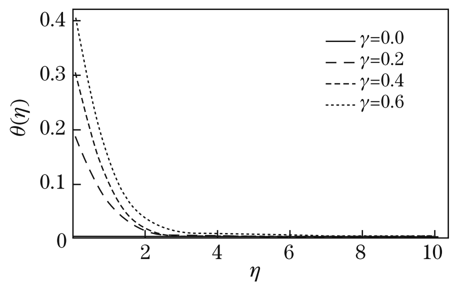

Fig. 13 Influence of γ on $\theta(\eta)$ when $\beta = 1.0$, $Pr = 1.0$, and $\beta_1 = \beta_2 = 0.4$

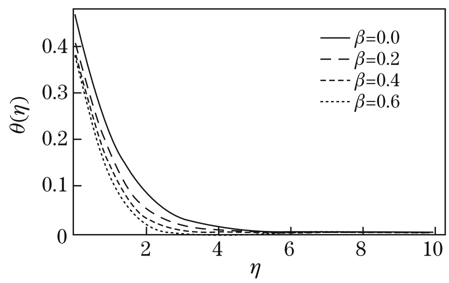

Fig. 14 Influence of β on $\theta(\eta)$ when $Pr = 1.0, \beta_1 = \beta_2 = 0.4$, and $\gamma = 0.6$

To see the convergent values of velocity and temperature, Table 1 is provided. From this Table, we make an argument that 20th-order deformations are enough for the convergent series solutions. Table 2 presents excellent agreement of series solutions with the existing exact and homotopy perturbation method (HPM) solutions for different values of β. Table 3 provides the numerical values of local Nusselt number for different values of β_1, β_2, Pr, and γ for $\beta=0.0$ and $\beta=0.5$. We notice that the values of the Nusselt number are small for $\beta=0.0$ in comparison to the values for $\beta=0.5$. This means that the values of the local Nusselt number increase with an increase in β.

Table 2 Comparison for different values of β by HAM, HPM, and exact solutions

β	HPM[29]		Exact[29]		HAM	
	$-f''(0)$	$-g''(0)$	$-f''(0)$	$-g''(0)$	$-f''(0)$	$-g''(0)$
0.0	1.000 00	0.000 00	1.000 000	0.000 000	1.000 00	0.000 00
0.1	1.020 25	0.066 84	1.020 259	0.066 847	1.020 26	0.066 85
0.2	1.039 49	0.148 73	1.039 495	0.148 736	1.039 49	0.148 74
0.3	1.057 95	0.243 35	1.057 954	0.243 359	1.057 95	0.243 36
0.4	1.075 78	0.349 20	1.075 788	0.349 208	1.075 78	0.349 21
0.5	1.093 09	0.465 20	1.093 095	0.465 204	1.093 09	0.465 21
0.6	1.109 94	0.590 52	1.109 946	0.590 528	1.109 94	0.590 53
0.7	1.126 39	0.724 53	1.126 397	0.724 531	1.126 39	0.724 53
0.8	1.142 48	0.866 68	1.142 488	0.866 682	1.142 49	0.866 68
0.9	1.158 25	1.016 53	1.158 253	1.016 538	1.158 26	1.016 54
1.0	1.173 72	1.173 72	1.173 720	1.173 720	1.173 72	1.173 72

Table 3 Values of local Nusselt number $-\theta'(0)$ for different values of parameters β_1, β_2, Pr, and γ

β_1	β_2	Pr	γ	$-\theta'(0)$	
				$\beta = 0.0$	$\beta = 0.5$
0.0	0.4	1.0	0.8	0.347 59	0.396 58
0.5	0.4	1.0	0.8	0.336 51	0.382 28
1.0	0.4	1.0	0.8	0.326 36	0.369 97
0.4	0.0	1.0	0.8	0.326 13	0.367 61
0.4	0.5	1.0	0.8	0.340 94	0.387 93
0.4	1.0	1.0	0.8	0.349 63	0.395 52
0.4	0.4	0.5	0.8	0.248 39	0.292 21
0.4	0.4	0.8	0.8	0.309 16	0.355 06
0.4	0.4	1.3	0.8	0.373 00	0.419 32
0.4	0.4	1.0	0.3	0.198 56	0.213 65
0.4	0.4	1.0	0.6	0.296 77	0.331 87
0.4	0.4	1.0	1.0	0.369 93	0.426 14

5 Conclusions

An analysis is presented for the three-dimensional flow of an Oldroyd-B fluid subject to convective type surface conditions. Series solutions are obtained for the velocity and temperature profiles. The main observations of this analysis are given below:

(i) The variations of the temperature by increasing β_1 are dominant for $\beta = 1.0$ in comparison to $\beta = 0.0$ and $\beta = 0.5$.

(ii) The fluid temperature and the thermal boundary layer thickness decrease rapidly for $\beta = 1.0$ when compared with $\beta = 0.0$ and $\beta = 0.5$.

(iii) The effects of the Biot number on the temperature and the thermal boundary layer thickness are quite similar for $\beta = 0.0$, $\beta = 0.5$, and $\beta = 1.0$.

(iv) The numerical values of the local Nusselt number increase as β increases.

(v) The values of the local Nusselt number are small for $\beta = 0.0$ in comparison with $\beta = 0.5$ (see Table 3).

Acknowledgements The authors are grateful to the reviewers for the useful suggestions.

References

[1] Jamil, M., Fetecau, C., and Imran, M. Unsteady helical flows of Oldroyd-B fluids. *Communications in Nonlinear Sciences and Numerical Simulation*, **16**, 1378–1386 (2011)

[2] Jamil, M. and Khan, N. A. Axial Couette flow of an Oldroyd-B fluid in an annulus. *Theoretical & Applied Mechanics Letters*, **2**, 012001 (2011)

[3] Sajid, M., Abbas, Z., Javed, T., and Ali, N. Boundary layer flow of an Oldroyd-B fluid in the region of stagnation point over a stretching sheet. *Canadian Journal of Physics*, **88**, 635–640 (2010)

[4] Hayat, T. and Alsaedi, A. On thermal radiation and Joule heating effects on MHD flow of an Oldroyd-B fluid with thermophoresis. *Arabian Journal of Science and Engineering*, **36**, 1113–1124 (2011)

[5] Hayat, T., Shehzad, S. A., Mustafa, M., and Hendi, A. A. MHD flow of an Oldroyd-B fluid through a porous channel. *International Journal of Chemical Reactor Engineering*, **10** (2012) DOI 10.1515/1542-6580.2655

[6] Sakiadis, B. C. Boundary layer behavior on continuous solid surfaces: I. boundary layer equations for two dimensional and axisymmetric flow. *AIChE Journal*, **7**, 26–28 (1961)

[7] Crane, L. J. Flow past a stretching plate. *Zeitschrift für Angewandte Mathematik und Physik*, **21**, 645–647 (1970)

[8] Sahoo, B. Effects of slip on sheet-driven flow and heat transfer of a non-Newtonian fluid past a stretching sheet. *Computers Mathematics with Applications*, **61**, 1442–1456 (2011)

[9] Mustafa, N., Asghar, S., and Hossain, M. A. Natural convection flow of second-grade fluid along a vertical heated surface with variable heat flux. *International Journal of Heat and Mass Transfer*, **53**, 5856–5862 (2010)

[10] Hayat, T., Shehzad, S. A., and Qasim, M. Mixed convection flow of a micropolar fluid with radiation and chemical reaction. *International Journal for Numerical Methods in Fluids*, **67**, 1418–1436 (2011)

[11] Makinde, O. D. and Aziz, A. MHD mixed convection from a vertical plate embedded in a porous medium with a convective boundary condition. *International Journal of Thermal Sciences*, **49**, 1813–1820 (2010)

[12] Bhattacharyya, K., Mukhopadhyay, S., and Layek, G. C. Slip effects on boundary layer stagnation-point flow and heat transfer towards a shrinking sheet. *International Journal of Heat and Mass Transfer*, **54**, 308–313 (2011)

[13] Fang, T. and Zhang, J. Thermal boundary layers over a shrinking sheet: an analytical solution. *Acta Mechanica*, **209**, 325–343 (2010)

[14] Rashidi, M. M., Pour, S. A. M., and Abbasbandy, S. Analytic approximate solutions for heat transfer of a micropolar fluid through a porous medium with radiation. *Communications in Nonlinear Sciences and Numerical Simulation*, **16**, 1874–1889 (2011)

[15] Hayat, T., Shehzad, S. A., Qasim, M., and Obaidat, S. Thermal radiation effects on the mixed convection stagnation-point flow in a Jeffery fluid. *Zeitschrift für Naturforschung A*, **66a**, 606–614 (2011)

[16] Yao, S., Fang, T., and Zhong, Y. Heat transfer of a generalized stretching/shrinking wall problem with convective boundary conditions. *Communications in Nonlinear Sciences and Numerical Simulation*, **16**, 752–760 (2011)

[17] Aziz, A. A similarity solution for thermal boundary layer over a flat plate with a convective surface boundary condition. *Communications in Nonlinear Sciences and Numerical Simulation*, **14**, 1064–1068 (2009)

[18] Hayat, T., Shehzad, S. A., Qasim, M., and Obaidat, S. Flow of a second grade fluid with convective boundary conditions. *Thermal Science*, **15**, S253–S259 (2011)

[19] Hayat, T., Shehzad, S. A., Qasim, M., and Obaidat, S. Steady flow of Maxwell fluid with convective boundary conditions. *Zeitschrift für Naturforschung A*, **66a**, 417–422 (2011)

[20] Makinde, O. D. and Aziz, A. Boundary layer flow of a nano fluid past a stretching sheet with convective boundary conditions. *International Journal of Thermal Sciences*, **50**, 1326–1332 (2011)

[21] Liao, S. J. *Beyond Perturbation*: *Introduction to Homotopy Analysis Method*, Chapman and Hall/CRC Press, Boca Raton (2003)

[22] Vosughi, H., Shivanian, E., and Abbasbandy, S. A new analytical technique to solve Volterra's integral equations. *Mathematical Methods in Applied Sciences*, **34**, 1243–1253 (2011)

[23] Yao, B. Approximate analytical solution to the Falkner-Skan wedge flow with the permeable wall of uniform suction. *Communications in Nonlinear Sciences and Numerical Simulation*, **14**, 3320–3326 (2009)

[24] Rashidi, M. M. and Pour, S. A. M. Analytic approximate solutions for unsteady boundary-layer flow and heat transfer due to a stretching sheet by homotopy analysis method. *Nonlinear Analysis*: *Modelling and Control*, **15**, 83–95 (2010)

[25] Iqbal, Z., Sajid, M., Hayat, T., and Obaidat, S. Flow and heat transfer with prescribed skin friction in a rotating fluid. *International Journal for Numerical Methods in Fluids*, **68**, 872–886 (2012)

[26] Hayat, T., Shehzad, S. A., Qasim, M., and Obaidat, S. Radiative flow of Jeffery fluid in a porus medium with power law heat flux and heat source. *Nuclear Engineering and Design*, **243**, 15–19 (2012)

[27] Harris, J. *Rheology and Non-Newtonian Flow*, Longman, London (1977)

[28] Schichting, H. *Boundary Layer Theory*, 6th ed., McGraw-Hill, New York (1964)

[29] Ariel, P. D. The three-dimensional flow past a stretching sheet and the homotopy perturbation method. *Computers Mathematics with Applications*, **54**, 920–925 (2007)